Inorganic Chemistry

Article

pubs.acs.org/IC

Coligand and Solvent Effects on the Architectures and Spin-Crossover Properties of (4,4)-Connected Iron(II) Coordination Polymers

Xue-Ru Wu,[†] Hai-Yan Shi,[†] Rong-Jia Wei,*[,†] Jia Li,[†] Lan-Sun Zheng,[†,‡] and Jun Tao*[,†,‡]

[†]State Key Laboratory of Physical Chemistry of Solid Surfaces and Department of Chemistry, College of Chemistry and Chemical Engineering and [‡]Collaborative Innovation Center of Chemistry for Energy Materials, Xiamen University, Xiamen 361005, People's Republic of China

Supporting Information

ABSTRACT: The self-assemblies of 1,4-bis(pyrid-4-yl)benzene (bpb) and $Fe(NCX)_2$ (X = S, Se, BH_3) afforded six coordination polymers with the general formula of $[Fe(bpb)_2(NCX)_2]\cdot Y$ (X = S and Y = $3C_2H_5OH\cdot 2.5H_2O$ for complex **4**, X = S and Y = $2C_2H_5OH$ for **5**, X = Se and Y = $2C_2H_5OH\cdot H_2O$ for **6**, X = Se and Y = $0.67CH_2Cl_2\cdot 1.33C_2H_5OH\cdot 0.67H_2O$ for **7**, X = BH_3 and Y = $3C_2H_5OH\cdot 2H_2O$ for **8**, X = BH_3 and Y = $2CH_2Cl_2\cdot 2C_2H_5OH$ for **9**). The frameworks of complexes **4** and **5** with the NCS^- anion as coligand are supramolecular isomers, of which complex **4** features a threefold self-interpenetrated three-dimensional (3D) $CdSO_4$-type topological structure with a Schläfli symbol of $6^5\cdot 8$, and complex **5** is a two-dimensional (2D) 4^4 rhombic grid network. These two complexes are purely high-spin systems. Complexes **6** and **7** with the $NCSe^-$ anion as coligand, both having the 3D $6^5\cdot 8$ $CdSO_4$-type framework, show gradual and incomplete spin-crossover behaviors with transition temperature $T_{1/2}$ being equal to 86 and 96 K, respectively. The usage of $NCBH_3^-$ anion as coligand leads to the formation of 2D 4^4 rhombic grid networks for both complexes **8** and **9**, which undergo relatively abrupt, complete spin crossover with $T_{1/2}$ being equal to 247 and 189 K, respectively. The structural divergences are attributed to the coligands NCX^- (X = S, Se, BH_3) and solvent molecules. Meanwhile, a significant coligand effect is observed on the spin-crossover behaviors of these complexes, and the completeness and transition temperature of spin-state conversion depends on the nature of the coligand, that is, $T_{1/2}(NCS^-) < T_{1/2}(NCSe^-) < T_{1/2}(NCBH_3^-)$. These results further facilitate the design and synthesis of spin-crossover complexes with spin-state conversion.

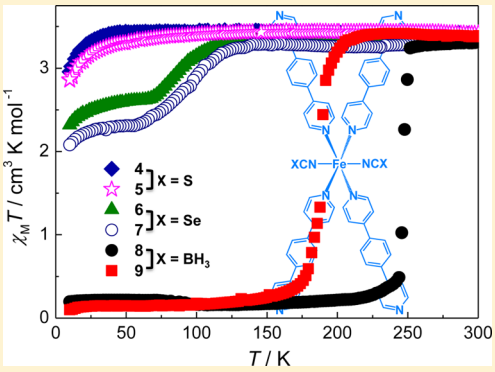

INTRODUCTION

Spin-crossover (SCO) complexes associated with electronic rearrangement of $3d^4-3d^7$ transition-metal ions (most commonly Fe^{II}) are well-known molecular switching materials.[1−3] The characteristic bistability arises from the switchable electronic configurations between the high-spin (HS) and the low-spin (LS) states in response to external perturbations driven by temperature gradients, pressure fluctuations, or light irradiation.[4−7] Frequently accompanying SCO, changes in magnetism, structure, and color usually happen, which may lead to potential technological applications in molecular switches, displays, and memory devices.[8−10] Whereas the early studies on SCO were focused on monounclear Fe^{II} complexes, recently more attention has been drawn in the design and synthesis of coordination polymers (CPs) incorporating SCO active centers in a framework that may enhance the communication through them and may thus result in abrupt and hysteretic spin-sate conversion.[11,12] The first polymeric SCO system belongs to the one-dimensional (1D) triazole-based complexes $[Fe(Htrz)_2(trz)]\cdot(BF_4)$ and $[Fe(4\text{-}Rtrz)_2]\cdot(anion)_2$ (trz^- is 1,2,4-triazolate anion, and R is the substituted group), some of which display large thermal hysteresis at high temperature.[13−15] Since then, more and more 1D, two-dimensional (2D), and three-dimensional (3D) polymeric SCO Fe^{II} complexes with a variety of bridging ligands based on triazoles,[16−19] tetrazoles,[20−24] and pyridines,[25−29] respectively, have been reported.

Among these SCO CPs, the system with the general formula $[FeL_2(NCX)_2]\cdot$solvent (X = S, Se, BH_3) is particularly important; it usually contains a distorted $[Fe^{II}N_6]$ octahedral unit that is formed by two N atoms from the trans-disposed monodentate anionic coligand (NCX^-) and four N atoms from the exo-bidentate linear bridging ligands (L), therefore allowing the (4,4)-connected topology to be the basic structural style for this system.[30−40] So far, polypyridine ligands that may exert suitable ligand-field strength on the metal centers are usually chosen as bridges to construct such SCO CPs. Meanwhile, long polypyridine ligands may generate porosities that provide spaces for solvent molecules to occupy within the frameworks. Therefore, the encapsulated solvent molecules could perturb the coordination environment of Fe^{II} centers and have a

Received: December 10, 2014
Published: March 30, 2015

DOI: 10.1021/ic5029542
Inorg. Chem. 2015, 54, 3773−3780

profound effect on tuning the ligand-field strength and thus the SCO behaviors.[30−35] For instance, complex $[Fe_2(azpy)_4(NCS)_4]\cdot$(guest) (azpy = *trans*-4,4′-azopyridine) featured a nanoporous, interpenetrated 2D rhombic grid network, which displayed a dramatic change in the SCO behavior upon guest absorption and desorption: the solvate form showed half SCO, whereas the desolvated form was in the temperature-independent HS state.[30] Similarly, 2D CP $[Fe(bpy)_2(NCS)_2]\cdot n$solvent (bpy = 4,4′-bipyridine) did not show SCO behavior when the solvent content was nitromethane, nitrobenzene, acetone, methanol, toluene, trichloroethene, carbon disulfide, or diethyl ether (n = 1−3);[41] however, SCO did occur when the solvent content was varied to $CHCl_3$.[42] Besides, the anionic coligand NCX^- coordinated to the Fe^{II} center also plays a significant role in affecting the SCO behavior, for example, the transition temperature, abruptness, completeness, etc.[6] Previous studies of mononuclear Fe^{II} complexes have shown the control of SCO behaviors by tuning the ligand-field strength of the "cyanide" coligand NCX^-,[43−51] whereas its effect in 2D and 3D CPs is relatively scarce.[38,39,52,53] In our previous studies, we reported the crystal structures and SCO properties of four isostructural CPs $[Fe(tppm)X_2]\cdot$solvent (tppm = 4,4′,4″,4‴-tetrakis(4-pyridylethen-2-yl)tetraphenylmethane and X = NCS^-, $NCSe^-$, $NCBH_3^-$, and $N(CN)_2^-$) based on a bulky tetradentate bridging ligand tppm and various anionic coligands, among which a remarkable SCO temperature shift was found in the transition temperature $T_{1/2}$, that is, $T_{1/2}(N(CN)_2^-) < T_{1/2}(NCS^-) < T_{1/2}(NCSe^-) < T_{1/2}(NCBH_3^-)$, which was concordant with the sequence of ligand-field strength of coligands.[53,54]

On the other hand, the synthetic and self-assembly processes of CPs are strongly related to various factors, such as metal ion, organic ligand, solvent, counterion, and temperature.[55−58] The variation of one or more conditions in one system may result in frameworks with different topological structures, that is, supramolecular isomers.[59−63] Thus, the accurate control of framework structure of CP in a self-assembly reaction is still a challenge.[64] We recently reported three CPs formulated as $[Fe(bpb)_2(NCS)_2]\cdot X$ [X = $3C_2H_5OH$ for **1**, $2.5H_2O$ for **2**, and 0 for **3**; bpb = 1,4-bis(pyrid-4-yl)benzene] whose framework structures were solvent-dependent. Complex **1** possessed a threefold self-interpenetrated 3D $6^5\cdot8$ $CdSO_4$-type framework structure, whereas complexes **2** and **3** were 2D 4^4 grid networks.[65] A solvent-mediated isomerization from complex **1** to **3** indicated that solvent molecules were critical to the self-assembly process of this system. In fact, attempts to change solvent medium for self-assembly have also afforded supramolecular isomers in other systems.[66−69] Taking into account the crucial roles of solvent molecules and anionic coligands, we are interested in further investigating how to modify them in the assembly of SCO CPs based on our previous work.[65] Here, we report the syntheses of six novel CPs with the general formula $[Fe(bpb)_2(NCX)_2]\cdot Y$, where X = S and Y = $3C_2H_5OH\cdot2.5H_2O$ for **4**, X = S and Y = $2C_2H_5OH$ for **5**, X = Se and Y = $2C_2H_5OH\cdot H_2O$ for **6**, X = Se and Y = $0.67CH_2Cl_2\cdot1.33C_2H_5OH\cdot0.67H_2O$ for **7**, X = BH_3 and Y = $3C_2H_5OH\cdot2H_2O$ for **8**, and X = BH_3 and Y = $2CH_2Cl_2\cdot2C_2H_5OH$ for **9** (Scheme 1). Their crystal structures and magnetic properties are detailedly studied, and the structure−property correlation in this system was also unveiled.

Scheme 1. Structural Unit of $[Fe(bpb)_2(NCX)_2]\cdot Y$

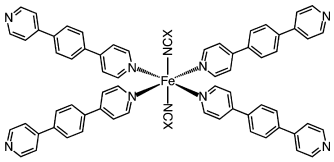

4: X = S, Y = $3C_2H_5OH\cdot2.5H_2O$
5: X = S, Y = $2C_2H_5OH$
6: X = Se, Y = $2C_2H_5OH\cdot H_2O$
7: X = Se, Y = $\frac{2}{3}CH_2Cl_2\cdot1\frac{1}{3}C_2H_5OH\cdot\frac{2}{3}H_2O$
8: X = BH_3, Y = $3C_2H_5OH\cdot2H_2O$
9: X = BH_3, Y = $2CH_2Cl_2\cdot2C_2H_5OH$

EXPERIMENTAL SECTION

Materials and Physical Measurements. All starting materials were purchased commercially and were used without further purification. Elemental analyses for C, H, and N were performed on a Vario EL III elemental analyzer. The IR spectra (KBr pellets) were recorded in the range 400−4000 cm^{-1} with an AVATAR330 FTIR spectrometer. Thermogravimetric analysis (TGA) was performed under nitrogen on a SDT Q600 thermobalance. Magnetic susceptibility measurements were carried out on a Quantum Design MPMS XL7 SQUID magnetometer at a sweeping rate of 1 K min^{-1} in the 10−300 K temperature range and under magnetic field of 0.5 T, freshly prepared sample was sealed in quartz tube with a small amount of mother liquor. Magnetic data were calibrated with the sample holder, and diamagnetic corrections were estimated from Pascal's constants.

$Fe(NCS)_2$, $Fe(NCSe)_2$, and $Fe(NCBH_3)_2$. A 5 mL ethanol solution of $FeSO_4\cdot7H_2O$ (1 mmol) was added to a solution of KNCS (2 mmol) in 5 mL ethanol and the resulting turbid solution was stirred for 15 min in nitrogen atmosphere. The precipitate (K_2SO_4) was filtered off and a colorless solution of $Fe(NCS)_2$ was obtained. $Fe(NCSe)_2$ and $Fe(NCBH_3)_2$ were prepared similarly with KNCSe and $NaNCBH_3$, respectively.

*$[Fe(bpb)_2(NCS)_2]\cdot3C_2H_5OH\cdot2.5H_2O$ (**4**).* An ethanol solution (8.5 mL) of $Fe(NCS)_2$ (0.05 mmol) was put in the bottom of a test tube, upon which an ethanol solution (3 mL) containing 0.1 mmol bpb was carefully layered at room temperature. Red crystals of complex **4** suitable for single-crystal X-ray diffraction studies crystallized out in 2 days. Yield: ca. 14 mg (34%). Anal. Calcd (%) for $C_{40}H_{47}FeN_6O_{5.5}S_2$: C, 58.60; H, 5.78; N, 10.25. Found: C, 58.96; H, 5.73; N, 9.97. IR (cm^{-1}): 3439(s), 2922(w), 2852(w), 2060(s), 1607(s), 1551(m), 1485(m), 1423(m), 1400(m), 1385(m), 1218(w), 1068(w), 1007(w), 808(s), 717(m), 579(w), 546(w), 486(w).

*$[Fe(bpb)_2(NCS)_2]\cdot2C_2H_5OH$ (**5**).* A dichloromethane/ethanol solution (6 mL, v:v = 1:1) of $Fe(NCS)_2$ (0.05 mmol) was put in the bottom of a test tube, an ethanol solution (5 mL) of bpb (0.1 mmol) was then layered upon. Red crystals of complex **5** were obtained in 2 days. Yield: ca. 13 mg (35%). Anal. Calcd (%) for $C_{38}H_{36}FeN_6O_2S_2$: C, 62.63; H, 4.98; N, 11.53. Found: C, 63.10; H, 5.12; N, 11.69. IR (cm^{-1}): 3448(m), 2062(s), 1605(s), 1549(m), 1483(m), 1425(m), 1400(m), 1215(w), 1066(w), 1005(w), 808(s), 716(m), 579(w), 488(w).

*$[Fe(bpb)_2(NCSe)_2]\cdot2C_2H_5OH\cdot H_2O$ (**6**).* Orange crystals of complex **6** were prepared in a similar method to that of complex **4** by using $Fe(NCSe)_2$. Yield: ca. 20 mg (48%). Anal. Calcd (%) for $C_{38}H_{38}FeN_6O_3Se_2$: C, 54.30; H, 4.56; N, 10.00. Found: C, 54.76; H, 4.32; N, 10.27. IR (cm^{-1}): 3435(s), 2923(w), 2856(w), 2051(m), 1606(s), 1576(m), 1486(w), 1423(m), 1398(m), 1109(s), 807(s), 716(w), 668(w), 577(w), 546(w).

*$[Fe(bpb)_2(NCSe)_2]\cdot0.67CH_2Cl_2\cdot1.33C_2H_5OH\cdot0.67H_2O$ (**7**).* Orange crystals of complex **7** were prepared in a similar method to that of complex **5** by using $Fe(NCSe)_2$. Yield: ca. 24 mg (56%). Anal. Calcd (%) for $C_{112}H_{104}Cl_4Fe_3N_{18}O_6Se_6$: C, 52.11; H, 4.06; N, 9.77. Found: C, 51.97; H, 4.10; N, 9.56. IR (cm^{-1}): 3437(s), 2922(w), 2854(w), 2046(m), 1654(m), 1604(s), 1560(s), 1419(m), 1129(w), 1067(w), 1006(w), 806(m), 715(m), 668(w), 618(w), 546(w), 496(w).

*$[Fe(bpb)_2(NCBH_3)_2]\cdot3C_2H_5OH\cdot2H_2O$ (**8**).* Yellow crystals of complex **8** were obtained accordingly to the synthetic method of complex **4** by using $Fe(NCBH_3)_2$. Yield: ca. 22 mg (57%). Anal. Calcd (%) for $C_{40}H_{52}B_2FeN_6O_5$: C, 62.04; H, 6.77; N 10.85. Found: C, 62.35; H, 6.42; N, 10.73. IR (cm^{-1}): 3438(s), 2922(w), 2348(m), 2181(s),

DOI: 10.1021/ic5029542
Inorg. Chem. 2015, 54, 3773−3780

Table 1. Crystal Data and Structural Refinement Parameters for Complexes 4−9

	4	5	6	7	8	9
T/K	153(2)	173(2)	153(2)	153(2)	153(2)	153(2)
formula	$C_{40}H_{47}FeN_6O_{5.5}S_2$	$C_{38}H_{36}FeN_6O_2S_2$	$C_{38}H_{38}FeN_6O_3Se_2$	$C_{112}H_{104}Cl_4Fe_3N_{18}O_6Se_6$	$C_{40}H_{52}B_2FeN_6O_5$	$C_{40}H_{46}B_2Cl_4FeN_6O_2$
M_r/g mol^{-1}	819.81	728.72	840.51	2581.24	774.35	841.25
space group	$C2/c$	$C2/c$	$C2/c$	$P2_1/c$	$P2_1/c$	$P2_1/c$
a/Å	22.077(2)	12.690(2)	22.110(3)	28.5702(13)	14.1404(8)	14.0894(6)
b/Å	13.7272(16)	15.807(2)	13.6595(14)	13.3980(7)	15.4361(5)	15.3990(5)
c/Å	15.0237(13)	18.999(3)	15.0436(14)	31.5549(14)	20.5104(8)	20.5520(8)
β/deg	115.814(9)	93.860(4)	116.019(10)	97.831(4)	103.704(4)	103.470(4)
V/Å^3	4098.7(7)	3802.4(10)	4082.8(7)	11966.1(10)	4349.4(3)	4336.4(3)
Z	4	4	4	4	4	4
D_{calcd}/g cm^{-3}	1.329	1.273	1.367	1.433	1.183	1.321
μ/mm^{-1}	4.321	0.547	5.329	6.252	3.152	5.379
reflns collected	7830	13 334	7052	34 989	15 380	15 857
$R1$ ($I > 2\sigma(I)$)	0.1308	0.0974	0.0982	0.1496	0.0760	0.0954
$wR2$ (all data)	0.3391	0.2690	0.2965	0.3884	0.2250	0.2956

1606(s), 1486(m), 1425(m), 1401(m), 1217(w), 1119(m), 1067(w), 1004(w), 858(w), 813(s), 804(s), 717(m), 580(w), 491(w).

*$[Fe(bpb)_2(NCBH_3)_2]\cdot 2CH_2Cl_2\cdot 2C_2H_5OH$ (**9**).* Yellow crystals of complex **9** were obtained accordingly to the synthetic method of complex **5** by using $Fe(NCBH_3)_2$. Yield: ca. 22 mg (53%). Anal. Calcd (%) for $C_{40}H_{46}B_2Cl_4FeN_6O_2$: C, 55.73; H, 5.38; N, 9.75. Found: C, 56.16; H, 5.44; N, 10.16. IR (cm^{-1}): 3448(s), 2927(w), 2346(m), 2181(m), 1606(s), 1577(s), 1560(s), 1486(w), 1420(m), 1227(w), 1120(w), 1004(w), 812(s), 716(w), 668(w), 579(w).

Desolvated samples were obtained by heating the as-synthesized complexes **4**−**9** at 90 °C under vacuum for 24 h.

Crystallographic Data Collection and Structure Determination. X-ray diffraction data were collected on Agilent SuperNova diffractometer using a Cu Kα radiation source (λ = 1.541 78 Å) and Rigaku IP diffractometer using graphite monochromated radiation Mo Kα (λ = 0.710 73 Å). Experimental absorption corrections were applied to all data. The structures were solved by direct methods and refined on F^2 by anisotropic full-matrix least-squares methods using SHELXL-97.[70] All non-hydrogen atoms were refined in the anisotropic approximation against F^2 for all reflections. Hydrogen-atom positions were calculated geometrically and were riding on their respective atoms. DELU and SIMU commands are applied during refinement to fix the ADP and disorder problems arising from the weak diffraction data for complex **4**, **6**, and **9**. For complex **9**, ISOR command is also used to fix the disorder of CH_2Cl_2 molecules. Electron density contributions from the highly disordered solvent molecules for complexes **4**, **6** ,and **7** were handled using the SQUEEZE procedure from the PLATON software.[71] Crystallographic data and structural refinement details are presented in Table 1, while selected bond lengths and parameters showing salient features of structures are summarized in Tables 2 and 3, respectively.

Table 2. Selected Bond Lengths and Structural Parameters of Complexes 4, 5, 8 and 9

	4	5	8	9
T/K	153(2)	173(2)	153(2)	153(2)
spin state	HS	HS	LS	LS
Fe−N_{eq}/Å	2.206(3)	2.192(6)	2.001(3)	1.997(5)
	2.206(3)	2.192(6)	2.001(3)	2.003(4)
	2.234(3)	2.214(8)	2.007(4)	2.004(5)
	2.234(3)	2.227(7)	2.007(3)	2.017(4)
Fe−N_{ax}/Å	2.103(7)	2.096(6)	1.935(4)	1.939(5)
	2.103(7)	2.096(6)	1.940(4)	1.939(5)
$\langle d_{Fe-N}\rangle^a$/Å	2.181	2.170	1.982	1.983
Fe−N−C(S/BH_3)/deg	153.8(14)	149.3(6)	175.6(4)	173.4(4)
	153.8(14)	149.3(6)	173.2(3)	172.0(4)
$\sum^b$/deg	17.6	21.7	8.0	8.7
grid size/Å^2	31.564 × 15.819	15.807 × 15.607	15.436 × 15.417	15.442 × 15.399
Fe···Fe distance between networks/Å	10.175	10.135	9.946	9.926
aperture size/Å^2	9.712 × 8.522	8.904 × 5.821	7.206 × 4.990	7.429 × 5.415
void space^c/Å^3	1261.2	1009.5	1765.0	1750.4

$^a\langle d_{Fe-N}\rangle$ is the average Fe−N bond length. ^{b}Distortion parameter $\sum$ is defined as the sum of absolute values of the deviations of the 12 *cis*-N−Fe−N angles from 90°. ^{c}The void space per unit cell is calculated by the SQUEEZE procedure from the PLATON software.

RESULTS AND DISCUSSION

Synthesis. A combination of NCX^- (X = S, Se, BH_3) coligands and solvents in the present system obviously influenced the framework structures of complexes **4**−**9** (see below). When NCS^- was used as coligand (as in complexes **4** and **5**), solvent molecules (ethanol) might contact with NCS^- via hydrogen bonding that affected the potential energy barriers for crystallization, which could lead to the formation of various framework isomers when the hydrogen bonds were disturbed (such as by dichloromethane in the synthesis of complex **5**), regardless of whether the solvent molecules (dichloromethane) were encapsulated or not. When the S atom in NCS^- was substituted with Se or BH_3, the changes in electronegativity and polarity could obviously reduce their ability to form hydrogen bonds with solvent molecules. Thus, solvent molecules exerted negligible effect on the framework structures of complexes **6**−**9**. Note that no coligand influence on the framework structures was found in the previously reported $[Fe(tppm)X_2]\cdot$solvent systems, and the complexes were isostructural.[53,54] In contrast, the framework structures of complexes **4**−**9** are obviously affected by the choice of coligand along with solvent molecules, showing interesting supramolecular isomerism. This may be due to the coordination flexibility of the (4,4)-connected grid-planar nodes, which have been reported to show different topologies.[65]

Crystallographic Studies. Single-crystal X-ray diffraction studies revealed that complexes **4**−**9** were constructed from the same structural unit $[Fe(bpb)_2(NCX)_2]$, where X = S for **4** and **5**, Se for **6** and **7**, and BH_3 for **8** and **9** (Scheme 1 and Figures S1−S7 in the Supporting Information). Each Fe^{II} atom adopts an octahedral $[FeN_6]$ coordination geometry that consists of

DOI: 10.1021/ic5029542
Inorg. Chem. 2015, 54, 3773−3780

Table 3. Selected Bond Lengths and Structural Parameters of Complexes 6 and 7

	6	7		
T/K	153(2)	153(2)		
spin state	HS	HS(Fe1)	HS(Fe2)	HS(Fe3)
Fe−N_{eq}/Å	2.220(4)	2.186(8)	2.209(8)	2.219(7)
	2.220(4)	2.229(9)	2.211(7)	2.232(8)
	2.222(5)	2.246(7)	2.213(8)	2.235(7)
	2.222(5)	2.250(7)	2.238(10)	2.238(8)
Fe−N_{ax}/Å	2.108(5)	2.072(10)	2.125(11)	2.079(9)
	2.108(5)	2.102(10)	2.126(10)	2.112(10)
$\langle d_{Fe-N}\rangle$/Å	2.183	2.181	2.187	2.186
Fe−N−C(Se)/deg	152.8(11)	152.9(9)	148.6(10)	167.6(9)
	152.8(11)	169.4(11)	170.5(11)	149.5(8)
$\sum$/deg	14.5	22.7	11.9	14.3
grid size/Å^2	31.576 × 15.755	31.555 × 15.848	31.654 × 15.819	
Fe···Fe distance between networks/Å	10.160	9.047		
aperture size/Å^2	9.613 × 8.481	7.795 × 7.310		
void space/Å^3	887.5	1601.3		

two axial NCX^- anions and four equatorial nitrogen atoms from the bpb ligands. The resulting four-connected, planar structural unit leads to the formation of 2D gridlike layer and 3D $CdSO_4$-type structures.

Complex **4** crystallized in the monoclinic space group $C2/c$ with the Fe^{II} ion in the asymmetric unit locating on an inversion center (Figure S1 in the Supporting Information). The solvent molecules within the lattice—three ethanol and two and a half water molecules per Fe^{II} unit revealed by elemental and thermogravimetric analyses—were highly disordered and could not be well-refined, and they were therefore removed when the structure was refined by using the SQUEEZE function.[71] As shown in Figure 1, the Fe^{II} ions are linked by the equatorial bpb bridges to form a 3D framework that corresponds to the $6^5{\cdot}8$ $CdSO_4$ topological structure with $[Fe_6(bpb)_6]$ rectangular motifs. The edge lengths of the $[Fe_6(bpb)_6]$ rectangle are 31.564 and 15.819 Å. This 3D framework possesses large void spaces, which are in fact occupied by two other identical frameworks, thus forming a triply self-interpenetrated structure with 1D open channels along the c axis allowing solvent molecules to reside (Figure 1). The closest Fe···Fe distance between adjacent frameworks is 10.175 Å. It should be mentioned here that the framework of complex **4** is strictly isostructural to that of complex **1**,[65] except that a difference between them is that both pyridyl groups of bpb ligand in **1** can rotate freely, while none of them (and the benzyl group) in complex **4** can. We speculate that the additional inclusion of water molecules in the 1D channels of complex **4** may fill the voids to the utmost so that no space lets pyridyl or benzyl group rotate. The Fe−N bond lengths at 153 K are in range of 2.103(7)−2.234(3) Å with an average value of 2.181 Å, indicating that Fe^{II} ion is in the HS state. It is well-known that the octahedral $[FeN_6]$ geometry is sensitive to the spin state of Fe^{II} ion and tends to be largely distorted in the HS state.[9,10] The variation has been quantified by using the octahedral distortion parameter $\sum$, defined by the sum of the deviation from 90° of the 12 *cis*-N−Fe−N angles.[72] For complex **4**, small distortion of the $[FeN_6]$ octahedron with a $\sum$ value of 17.6° is observed (Table 2), which, however, is relevant to an HS state of the Fe^{II} ion (small $\sum$ value usually refers to LS state of Fe^{II} ion).

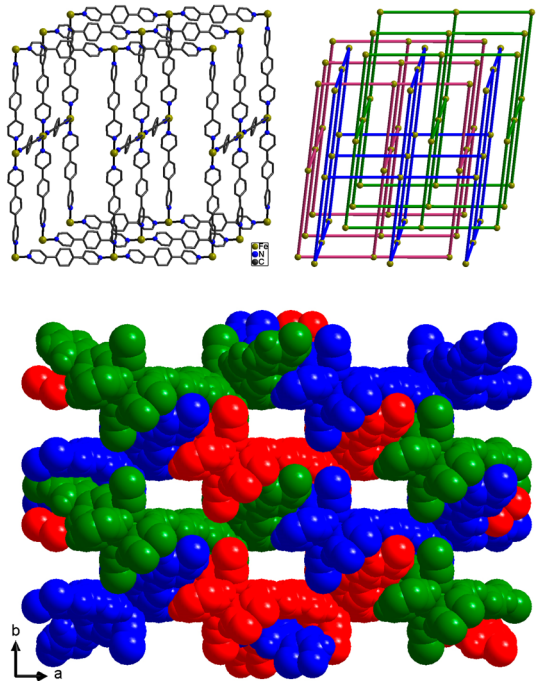

Figure 1. Perspective view of the 3D $CdSO_4$-type framework structure (upper left), topological representation of the threefold self-interpenetrated structure (upper right), and space-filling pattern (lower) of complex **4**. Hydrogen atoms, anionic coligand NCS^-, and lattice solvent molecules are omitted for clarity.

The asymmetric unit of complex **5** contains a complete $[Fe(bpb)_2(NCS)_2]$ unit and two ethanol molecules. The Fe^{II} sites are linked by the equatorial bpb ligands to form a 2D gridlike layer in the bc plane (Figure 2), in which the Fe···Fe distances through the bpb bridges are 15.807 and 15.607 Å. Such layers are stacked in an ABAB style, forming 1D channels running along the a axis that are occupied by solvent molecules (Figure 2). The shortest interlayer Fe···Fe distance is 10.135 Å. The average Fe−N distance is 2.170 Å at 173 K, a typical value for an HS Fe^{II} ion. The Fe−N_{bpb} bond lengths, in the range from 2.192(6) to 2.227(7) Å, are slightly longer than those of the Fe−N_{NCS} bond lengths (2.096(6) Å). The $\sum$ value of 21.7° is larger than that of complex **4**, which accompanying with the Fe−N bond lengths also indicates an HS state of the Fe^{II} site.

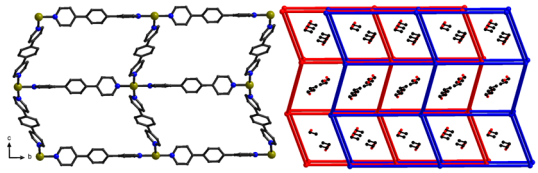

Figure 2. 2D gridlike structure (left) and ABAB stacking pattern of complex **5**. Hydrogen atoms and anionic coligand NCS^- are omitted for clarity.

The framework structure of complex **6** is strictly isostructural to that of complex **4** (Figure 1), in which the coligand NCS^- (complex **4**) was replaced with $NCSe^-$ for complex **6**. The Fe−N bond lengths range from 2.108(5) to 2.222(5) Å with an

DOI: 10.1021/ic5029542
Inorg. Chem. 2015, 54, 3773−3780

average value of 2.183 Å, which is in the range expected for an HS Fe^{II}–N bond.

The structure of complex **7** is also a threefold interpenetrated 3D $6^5{\cdot}8$ $CdSO_4$-type framework, similar to those of complexes **4** and **6**, but showing more distorted $[Fe_6(bpb)_6]$ rectangular motifs (Figure 3). In the asymmetric unit, there are two

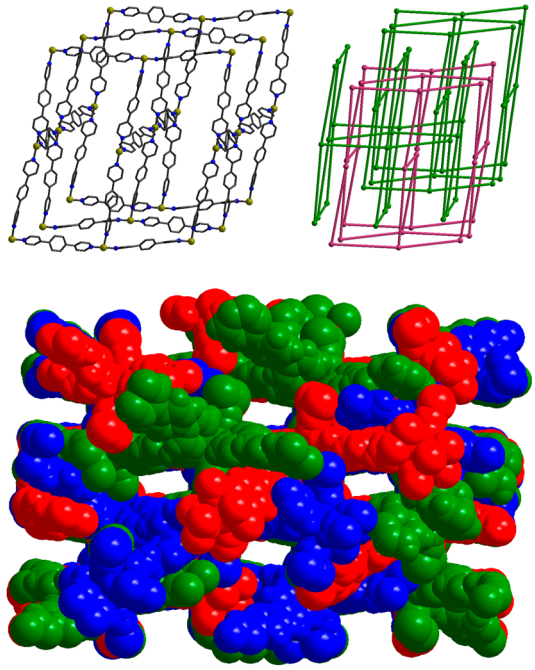

Figure 3. Perspective view of the 3D $CdSO_4$-type framework structure (upper left), topological representation of the threefold self-interpenetrated structure (upper right), and space-filling pattern (lower) of complex **7**. Hydrogen atoms, anionic coligand $NCSe^-$, and lattice solvent molecules are omitted for clarity.

$[Fe(bpb)_2(NCSe)_2]$ structural units—one with the Fe1 ion and another one with Fe2 and Fe3 ions (Figures S4 and S5 in the Supporting Information)—and in addition two dichloromethane, four ethanol, and two water molecules per asymmetric unit (three Fe^{II} ions) in the lattice are indicated by the difference density map and elemental and thermogravimetric analyses. The adjacent Fe1 ions are connected by bpb ligands to form 3D $6^5{\cdot}8$ $CdSO_4$-type framework with highly distorted $[Fe_6(bpb)_6]$ rectangular motifs with edges being 31.555 and 15.848 Å, respectively. The large spaces within the framework are occupied by two other independent $CdSO_4$-type frameworks that are formed from the Fe2/Fe3 structural units, therefore achieving a threefold interpenetrated 3D framework with 1D channels encapsulating solvent molecules (Figure 3). All Fe^{II} ions are in HS states with average Fe–N bond lengths of 2.181, 2.186, and 2.187 Å for Fe1, Fe2, and Fe3 sites, respectively. The $\sum$ values (Table 2) are 22.7°, 14.3°, and 11.9° for Fe1, Fe2, and Fe3 coordination octahedra, respectively, also related to the HS state for all Fe^{II} ions.

Complexes **8** and **9** crystallize in the monocline space group $P2_1/c$, showing isostructural frameworks with the same structural unit $[Fe(bpb)_2(NCBH_3)_2]$. The solvent molecules in the asymmetric units are three ethanol and two water molecules for complex **8** and two dichloromethane and two ethanol molecules for complex **9**. The 2D 4^4 rhombic grid networks with sizes of 15.417 × 15.436 and 15.399 × 15.442 $Å^2$ for complexes **8** and **9**, respectively, are stacked in an ABAB manner in the *bc* plane (Figure 4), generating 1D channels where solvent molecules reside. The shortest interlayer Fe···Fe distances are 9.946 and 9.926 Å for complexes **8** and **9**, respectively. At 153 K, the Fe^{II} ions in complexes **8** and **9** persist in the LS state with average Fe–N bond lengths of 1.982 and 1.983 Å, respectively. The $\sum$ values of 8.0° and 8.7° for complexes **8** and **9** (Table 2), respectively, are obviously smaller than those of complexes **4**–**6**, consistent with their spin states of Fe^{II} ions. It is also worth noting that the Fe–N–$C(BH_3)$ bond angles with values of 175.6(4)° and 173.2(4)° for complex **8** and 173.4(4)° and 172.0(4)° for complex **9** are more closer to 180° than the Fe_{HS}–N–C(S) bond angles in complexes **4** and **5** and Fe_{HS}–N–C(Se) bond angles in complexes **6** and **7** (Tables 2 and 3). So far, the Fe–N–C(X) bond angle has been proven to show large deviation from 180° for HS Fe^{II} ion.[41] Hence, the considerable regular linear Fe–N–$C(BH_3)$ bond angle may help to stabilize the LS state of Fe^{II} ions in complexes **8** and **9**. When they were warmed to 230 K, the crystals of complexes **8** and **9** showed dramatic color changes from red to yellow, indicating the occurrence of LS-to-HS spin transitions of the Fe^{II} ions (Figures S15 and S16 in the Supporting Information). However, we could not collect high-quality diffraction data of complexes **8** and **9** at this temperature despite many attempts, and therefore the crystal structures of complexes **8** and **9** at 230 K could not be solved, which may be due to the loss of solvent molecules and/or phase transition.

Magnetic Properties. The thermally dependent $\chi_M T$ values of complexes **4**–**9** are plotted in Figure 5, where χ_M is the molar magnetic susceptibility and T is the temperature. The magnetic measurements were performed using freshly prepared

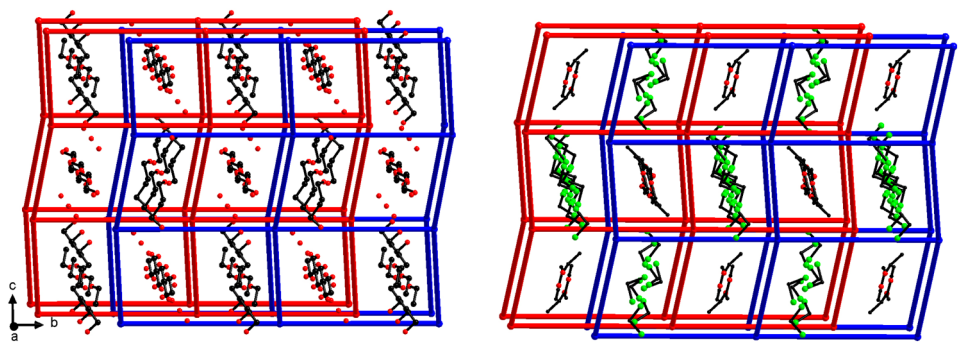

Figure 4. ABAB stacking patterns of complexes **8** (left) and **9** (right), respectively, viewed along the *a* axis with lattice solvent molecules. Hydrogen atoms and anionic coligand $NCBH_3^-$ are omitted for clarity.

DOI: 10.1021/ic5029542
Inorg. Chem. 2015, 54, 3773–3780

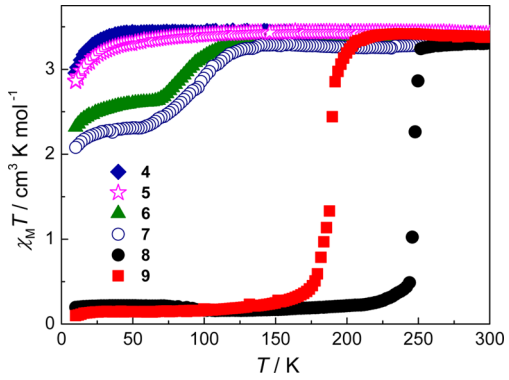

Figure 5. $\chi_M T$ vs T plots for complexes **4**–**9**.

crystalline samples with a small amount of mother liquor to prevent desolvation of the samples.

The $\chi_M T$ values at 300 K for complexes **4** and **5** (coligand is NCS^-) are 3.39 and 3.42 cm^3 K mol^{-1}, respectively, being typical values for octahedral HS Fe^{II} ions.[73] The $\chi_M T$ values remain constant when the crystals are cooled until sudden decreases occur below 25 K that are possibly due to the zero-field splitting effects of HS Fe^{II} ions, which suggest that complexes **4** and **5** are paramagnetic in the whole temperature range. As for complexes **6** and **7** (coligand is $NCSe^-$), the $\chi_M T$ values are 3.32 and 3.35 cm^3 K mol^{-1}, respectively, at 300 K, which are indicative of HS Fe^{II} ions. When the crystals are cooled to 116 K, the $\chi_M T$ value of **6** begins to decrease and reaches a plateau of 2.66 cm^3 K mol^{-1} between 70 and 25 K, thus indicating SCO behavior with $T_{1/2}$ being ca. 82 K, whereas complex **7** shows a similar temperature-dependent behavior with $T_{1/2}$ being 96 K. Both magnetic properties of complexes **6** and **7** indicate that they only undergo incomplete SCO. Note that the low-temperature $\chi_M T$ value for complex **7** is lower than that of complex **6**, so we can conclude that complex **7** remains smaller residual HS fraction at low temperature.

Complexes **8** and **9** (coligand is $NCBH_3^-$) are also in HS states at room temperature with the $\chi_M T$ values of 3.32 and 3.39 cm^3 K mol^{-1}, respectively. But when temperature decreases, complexes **8** and **9** undergo abrupt, complete SCO. For complex **8**, the $\chi_M T$ value drops sharply from 252 to 240 K, then reaches a value of 0.20 cm^3 K mol^{-1} at 10 K, while for complex **9**, the $\chi_M T$ value begins to drop from 206 K and attains 0.33 cm^3 K mol^{-1} at 175 K. The $T_{1/2}$ values can be estimated to be ca. 247 and 189 K for complexes **8** and **9**, respectively. Magnetic susceptibility measurements in multiple down–up cycles are also performed for complexes **6**–**9** (Figure S22–25, Supporting Information). However, no hysteresis accompanying the SCO is found.

We also investigated the magnetic properties of fully desolvated forms of complexes **6**–**9**, which show that all desolvated samples are stabilized at paramagnetic HS states (Figures S18–S21, Supporting Information).

Chemical Perturbation on Spin Crossover. First, the SCO behaviors of complexes **6**–**9** must be sensitive to the nature of encapsulated solvent molecules. It is well-known that protic solvents such as ethanol and water can effectively stabilize the HS state of Fe^{II} ion with NCS^- coligand, which consequently favors lowering the SCO transition temperature ($T_{1/2}$).[30,54,74] But in the cases of complexes **8** and **9**, the replacement of ethanol with dichloromethane results in an obvious decrease of $T_{1/2}$ value from 247 K (**8**) to 189 K (**9**); the reason for this may be that when $NCBH_3^-$ acts as coligand the hydrogen bonds between ethanol/water and $NCBH_3^-$ are not strong enough to dominate the transition temperature, so that other factors such as polarity (P) or van der Waals volume (V)[7,31,32,53,54] may play more crucial role ($P_{dichloromethane} < P_{ethanol}$, $V_{dichloromethane} > V_{ethanol}$).[75]

On the other hand, the magnetic properties of complexes **4**–**9** are drastically relevant to the coligand NCX^- (X = S, Se, or BH_3). Along with the increasing of ligand-field strength from NCS^- to $NCSe^-$ and to $NCBH_3^-$, complexes **4** and **5** show temperature-independent HS states, complexes **6** and **7** undergo incomplete, gradual SCO, and complexes **8** and **9** display complete, abrupt SCO with higher transition temperature. The coligand effect on SCO in present case is similar but more obvious than that of $[Fe(tppm)X_2]\cdot$solvent systems, of which the $T_{1/2}$ values shifted to higher temperature range along with the alteration of stronger ligand-field anionic coligands.[53,54] These results are consistent with those revealed by theoretical and experimental methods.[53,76] It should be also mentioned that supramolecular isomeric structures may influence the SCO behaviors.[8,77,78] However, because of the lack of supramolecular 2D isomers for complexes **6** and **7** and supramolecular 3D isomers for complexes **8** and **9** at present, the effect of isomeric structure on SCO behaviors in system of $[Fe(bpb)_2(NCX)_2]$ is not yet clear.

CONCLUSION

We have reported six Fe^{II} complexes based on rigid linear bpb "spacers" and square planar $[Fe(NCX)_2]$ "nodes" (X = S, Se, BH_3); their framework structures and magnetic properties are affected by anionic coligands and solvent molecules. These complexes crystallize in two different structural motifs, that is, threefold self-interpenetrated 3D $6^5{\cdot}8$ $CdSO_4$-type frameworks for complexes **4**, **6**, and **7** and 2D 4^4 rhombus-grid networks for complexes **5**, **8**, and **9**. In particular, the variation of solvent medium affords different topological structures for complexes **4** and **5** (both with coligand NCS^-), which indicate the formation of supramolecular isomers that originate from solvent effects. However, this effect is weakened and even negligible upon the formation of complexes **6**–**9**. Complexes **8** and **9** with coligand $NCBH_3^-$ of the strongest ligand field show complete, abrupt HS↔LS spin-state conversions, whose critical temperatures ($T_{1/2}$) are higher than those of complexes **6** and **7** with coligand $NCSe^-$, which only undergo incomplete and gradual SCO. Complexes **4** and **5** with coligand NCS^- are paramagnetic in whole temperature range. The results show that the $[Fe(bpb)_2(NCX)_2]$ entity is a suitable system for the investigation of coligand and solvent effects on the self-assembly process and SCO behaviors.

ASSOCIATED CONTENT

Supporting Information

Crystal data in CIF format and figures, details of SQUEEZE, checkcif explanation, illustrated structural units, TGA, IR spectra, color changes of complexes **8** and **9**, magnetic properties of desolvated complexes, $\chi_M T$ versus T plots. This material is available free of charge via the Internet at http://pubs.acs.org.

AUTHOR INFORMATION

Corresponding Authors

*E-mail: rongjiawei@126.com. (R.J.W.)
*E-mail: taojun@xmu.edu.cn. (J.T.)

DOI: 10.1021/ic5029542
Inorg. Chem. 2015, 54, 3773–3780

Notes

The authors declare no competing financial interest.

■ ACKNOWLEDGMENTS

This work was supported by the National Natural Science Foundation of China (Grant No. 21325103), the National Key Basic Research Program of China (973 Project, Grant No. 2014CB845601), and the Specialized Research Fund for the Doctoral Program of Higher Education (Grant No. 20110121110012).

■ REFERENCES

(1) Kahn, O.; Martinez, C. J. *Science* **1998**, *279*, 44−48.
(2) Kahn, O. *Chem. Br.* **1999**, *35*, 24−27.
(3) Shultz, D. A. In *Magnetism: Molecules to Materials II*; Miller, J. S.; Drillon, M., Eds.; Wiley-VCH: Weinheim, Germany, 2001; p 281.
(4) Sato, O.; Tao, J.; Zhang, Y.-Z. *Angew. Chem., Int. Ed.* **2007**, *46*, 2152−2187.
(5) Tao, J.; Maruyama, H.; Sato, O. *J. Am. Chem. Soc.* **2006**, *128*, 1790−1791.
(6) Gütlich, P.; Goodwin, H. A. *Top. Curr. Chem.* **2004**, *234*, 1−27.
(7) Gütlich, P.; Garcia, Y.; Goodwin, H. A. *Chem. Soc. Rev.* **2000**, *29*, 419−427.
(8) Tao, J.; Wei, R.-J.; Huang, R.-B.; Zheng, L.-S. *Chem. Soc. Rev.* **2012**, *41*, 703−737.
(9) Li, B.; Wei, R.-J.; Tao, J.; Huang, R.-B.; Zheng, L.-S.; Zheng, Z. *J. Am. Chem. Soc.* **2010**, *132*, 1558−1566.
(10) Wei, R.-J.; Huo, Q.; Tao, J.; Huang, R.-B.; Zheng, L.-S. *Angew. Chem., Int. Ed.* **2011**, *50*, 8940−8943.
(11) Létard, J. F.; Guionneau, P.; Goux-Capes, L. *Top. Curr. Chem.* **2004**, *235*, 221−249.
(12) Murray, K. S.; Kepert, C. J. *Top. Curr. Chem.* **2004**, *233*, 195−228.
(13) Haasnoot, J. G.; Vos, J. G.; Groeneveld, W. L. *Z. Naturforsch., B* **1977**, *32*, 1421−1430.
(14) Michalowicz, A.; Moscovici, J.; Ducourant, B.; Craco, D.; Kahn, O. *Chem. Mater.* **1995**, *7*, 1833−1842.
(15) Kröber, J.; Audière, R.; Claude, R.; Codjovi, E.; Kahn, O.; Haasnoot, J. G.; Groliere, F.; Jay, C.; Bousseksou, A.; Linares, J.; Varret, F.; Gonthier-Vassal, A. *Chem. Mater.* **1994**, *6*, 1404−1412.
(16) Bronisz, R. *Inorg. Chem.* **2005**, *44*, 4463−4465.
(17) Legrand, V.; Pillet, S.; Carbonera, C.; Souhassou, M.; Letard, J.-F.; Guionneau, P.; Lecomte, C. *Eur. J. Inorg. Chem.* **2007**, 5693−5706.
(18) Garcia, Y.; Kahn, O.; Rabardel, L.; Chansou, B.; Salmon, L.; Tuchagues, J. *Inorg. Chem.* **1999**, *38*, 4663−4670.
(19) Grunert, C. M.; Schweifer, J.; Weinberger, P.; Linert, W.; Mereiter, K.; Hilscher, G.; Müller, M.; Wiesinger, G.; van Koningsbruggen, P. J. *Inorg. Chem.* **2004**, *43*, 155−165.
(20) van Koningsbruggen, P. J.; Garcia, Y.; Kooijman, H.; Spek, A. L.; Haasnoot, J. G.; Kahn, O.; Linares, J.; Codjovi, E.; Varret, F. *J. Chem. Soc., Dalton Trans.* **2001**, 466−471.
(21) Grunert, C. M.; Schweifer, J.; Weinberger, P.; Linert, W.; Mereiter, K.; Hilscher, G.; Müller, M.; Wiesinger, G.; van Koningsbruggen, P. J. *Inorg. Chem.* **2004**, *43*, 155−165.
(22) Bronisz, R. *Inorg. Chem.* **2007**, *46*, 6733−6739.
(23) Bialonska, A.; Bronisz, R.; Weselski, M. *Inorg. Chem.* **2008**, *47*, 4436−4438.
(24) Quesada, M.; Kooijman, H.; Gamez, P.; Costa, J. S.; van Koningsbruggen, P. J.; Weinberger, P.; Reissner, M.; Spek, A. L.; Haasnoot, J. G.; Reedijk, J. *Dalton Trans.* **2007**, 5434−5440.
(25) Quesada, M.; de la Peña-O'Shea, V. A.; Aromí, G.; Geremia, S.; Massera, C.; Roubeau, O.; Gamez, P.; Reedijk, J. *Adv. Mater.* **2007**, *19*, 1397−1401.
(26) Bao, X.; Liu, J.-L.; Leng, J.-D.; Lin, Z.; Tong, M.-L.; Nihei, M.; Oshio, H. *Chem.−Eur. J.* **2010**, *16*, 7973−7978.
(27) Niel, V.; Thompson, A. L.; Muñoz, M. C.; Galet, A.; Goeta, A. E.; Real, J. A. *Angew. Chem., Int. Ed.* **2003**, *42*, 3760−3763.
(28) Galet, A.; Niel, V.; Muñoz, M. C.; Real, J. A. *J. Am. Chem. Soc.* **2003**, *125*, 14224−14225.
(29) Muñoz, M. C.; Real, J. A. *Coord. Chem. Rev.* **2011**, *255*, 2068−2093.
(30) Halder, G. J.; Kepert, C. J.; Moubaraki, B.; Murray, K. S.; Cashion, J. D. *Science* **2002**, *298*, 1762−1765.
(31) Halder, G. J.; Chapman, K. W.; Neville, S. M.; Moubaraki, B.; Murray, K. S.; Létard, J.-F.; Kepert, C. J. *J. Am. Chem. Soc.* **2008**, *130*, 17552−17562.
(32) Neville, S. M.; Halder, G. J.; Chapman, K. W.; Duriska, M. B.; Southon, P. D.; Cashion, J. D.; Létard, J.-F.; Moubaraki, B.; Murray, K. S.; Kepert, C. J. *J. Am. Chem. Soc.* **2008**, *130*, 2869−2876.
(33) Neville, S. M.; Moubaraki, B.; Murray, K. S.; Kepert, C. J. *Angew. Chem., Int. Ed.* **2007**, *46*, 2059−2063.
(34) Southon, P. D.; Liu, L.; Fellows, E. A.; Price, D. J.; Halder, G. J.; Chapman, K. W.; Moubaraki, B.; Murray, K. S.; Létard, J.-F.; Kepert, C. J. *J. Am. Chem. Soc.* **2009**, *131*, 10998−11009.
(35) Neville, S. M.; Halder, G. J.; Chapman, K. W.; Duriska, M. B.; Moubaraki, B.; Murray, K. S.; Kepert, C. J. *J. Am. Chem. Soc.* **2009**, *131*, 12106−12108.
(36) Moliner, N.; Muñoz, M. C.; Letard, S.; Solans, X.; Menendez, N.; Goujon, A.; Varret, F.; Real, J. A. *Inorg. Chem.* **2000**, *39*, 5390−5393.
(37) Real, J. A.; Andres, E.; Muñoz, M. C.; Julve, M.; Granier, T.; Bousseksou, A.; Varret, F. *Science* **1995**, *268*, 265−267.
(38) Vreugdenhil, W.; Van Diemen, J. H.; De Graaff, R. A. G.; Haasnoot, J. G.; Reedijk, J.; Van Der Kraan, A. M.; Kahn, O.; Zarembowitch, J. *Polyhedron* **1990**, *9*, 2971−2979.
(39) Ozarowski, A.; Shunzhong, Y.; McGarvey, B. R.; Mislankar, A.; Drake, J. E. *Inorg. Chem.* **1991**, *30*, 3167−3174.
(40) Li, J.-Y.; Yan, Z.; Ni, Z.-P.; Zhang, Z.-M.; Chen, Y.-C.; Liu, W.; Tong, M.-L. *Inorg. Chem.* **2014**, *53*, 4039−4046.
(41) Adams, C. J.; Real, J. A.; Waddington, R. E. *CrystEngComm* **2010**, *12*, 3547−3553.
(42) Adams, C. J.; Muñoz, M. C.; Waddington, R. E.; Real, J. A. *Inorg. Chem.* **2011**, *50*, 10633−10642.
(43) Moliner, N.; Muñoz, M. C.; Letard, S.; Solans, X.; Menendez, N.; Goujon, A.; Varret, F.; Real, J. A. *Inorg. Chem.* **2000**, *39*, 5390−5393.
(44) Moliner, N.; Gaspar, A. B.; Muñoz, M. C.; Niel, V.; Cano, J.; Real, J. A. *Inorg. Chem.* **2001**, *40*, 3986−3991.
(45) Moliner, N.; Muñoz, M. C.; Létard, S.; Létard, J.-F.; Solans, X.; Burriel, R.; Castro, M.; Kahn, O.; Real, J. A. *Inorg. Chim. Acta* **1999**, *291*, 279−288.
(46) Kunkeler, P. J.; van Koningsbruggen, P. J.; Cornelissen, J. P.; van der Horst, A. N.; van der Kraan, A. M.; Spek, A. L.; Haasnoot, J. G.; Reedijk, J. *J. Am. Chem. Soc.* **1996**, *118*, 2190−2197.
(47) Scott, H. S.; Ross, T. M.; Chilton, N. F.; Gass, I. A.; Moubaraki, B.; Chastanet, G.; Paradis, N.; Létard, J.-F.; Vignesh, K. R.; Rajaraman, G.; Batten, S. R.; Murray, K. S. *Dalton Trans.* **2013**, *42*, 16494−16509.
(48) Klingele, J.; Kaase, D.; Klingele, M. H.; Lach, J. *Dalton Trans.* **2012**, *41*, 1397−1406.
(49) Cirea, J.; Paesani, F. *Inorg. Chem.* **2012**, *51*, 8194−8201.
(50) Hogue, R. W.; Miller, R. G.; White, N. G.; Feltham, H. L. C.; Jameson, G. N. L.; Brooker, S. *Chem. Commun.* **2014**, *50*, 1435−1437.
(51) Halcrow, M. A. *Chem. Commun.* **2013**, *4* (9), 10890−10892.
(52) Morita, T.; Nakashima, S.; Yamada, K.; Inoue, K. *Chem. Lett. 1042*, 1043−1044.
(53) Chen, X.-Y.; Huang, R.-B.; Zheng, L.-S.; Tao, J. *Inorg. Chem.* **2014**, *53*, 5246−5252.
(54) Chen, X.-Y.; Shi, H.-Y.; Huang, R.-B.; Zheng, L.-S.; Tao, J. *Chem. Commun.* **2013**, *49*, 10977−10979.
(55) Zaworotko, M. J. *Chem. Commun.* **2001**, 1−9.
(56) Moulton, B.; Zaworotko, M. J. *Chem. Rev.* **2001**, *101*, 1629−1658.
(57) Hennigar, T. L.; MacQuarrie, D. C.; Losier, P.; Rogers, R. D.; Zaworotko, M. J. *Angew. Chem., Int. Ed. Engl.* **1997**, *36*, 972−973.

DOI: 10.1021/ic5029542
Inorg. Chem. 2015, 54, 3773−3780

(58) Schröder, M.; Champness, N. R. In *Encyclopedia of Supramolecular Chemistry;* Atwood, J. L., Steed, P., Eds; Marcel Dekker, Inc.: New York, 2004; p 1420−1426.
(59) Hu, C.; Englert, U. *Angew. Chem., Int. Ed.* **2005**, *44*, 2281−2283.
(60) Zhang, J.-P.; Lin, Y.-Y.; Zhang, W.-X.; Chen, X.-M. *J. Am. Chem. Soc.* **2005**, *127*, 14162−14165.
(61) Noro, S.-I.; Kitaura, R.; Kondo, M.; Kitagawa, S.; Ishii, T.; Matsuzaka, H.; Yamashita, M. *J. Am. Chem. Soc.* **2002**, *124*, 2568−2582.
(62) Biradha, K.; Hongo, Y.; Fujita, M. *Angew. Chem., Int. Ed.* **2002**, *41*, 3395−3398.
(63) Min, K. S.; Suh, M. P. *J. Am. Chem. Soc.* **2000**, *122*, 6834−6840.
(64) Zhang, J.-P.; Huang, X.-C.; Chen, X.-M. *Chem. Soc. Rev.* **2009**, *38*, 2385−2396.
(65) Wu, X.-R.; Yang, X.; Wei, R.-J.; Li, J.; Zheng, L.-S.; Tao, J. *Cryst. Growth Des.* **2014**, *14*, 4891−4894.
(66) Kawano, M.; Fujita, M. *Coord. Chem. Rev.* **2007**, *251*, 2592−2605.
(67) Vittal, J. J. *Coord. Chem. Rev.* **2007**, *251*, 1781−1795.
(68) Fu, A.-Y.; Jiang, Y.-L.; Wang, Y.-Y.; Gao, X.-N.; Yang, G.-P.; Hou, L.; Shi, Q.-Z. *Inorg. Chem.* **2010**, *49*, 5495−5502.
(69) Li, C.-P.; Chen, J.; Liu, P.-W.; Du, M. *CrystEngComm* **2013**, *15*, 9713−9721.
(70) Sheldrick, G. M. *Acta Crystallogr.* **2008**, *A64*, 112−122.
(71) Spek, A. L. *Acta Crystallogr.* **2009**, *D65*, 148−155.
(72) Halcrow, M. A. *Chem. Soc. Rev.* **2011**, *40*, 4119−4142.
(73) Kahn, O. *Molecular Magnetism;* Wiley-VCH: New York, 1993.
(74) Brewer, C. T.; Brewer, G.; Butcher, R. J.; Carpenter, E. E.; Schmiedekamp, A. M.; Schmiedekamp, C.; Straka, A.; Viragh, C.; Yuzefpolskiy, Y.; Zavalij, P. *Dalton Trans.* **2011**, *40*, 181−194.
(75) Smallwood, I. M. *Handbook of Organic Solvent Properties;* Hodder Headline Group: London, U.K., 1996.
(76) Cirea, J.; Paesani, F. *Inorg. Chem.* **2012**, *51*, 8194−8201.
(77) Yan, Z.; Li, M.; Gao, H.-L.; Huang, X.-C.; Li, D. *Chem. Commun.* **2012**, *48*, 3960−3962.
(78) Yan, Z.; Ni, Z.-P.; Guo, F.-S.; Li, J.-Y.; Chen, Y.-C.; Liu, J.-L.; Lin, W.-Q.; Aravena, D.; Ruiz, E.; Tong, M.-L. *Inorg. Chem.* **2014**, *53*, 201−208.

DOI: 10.1021/ic5029542
Inorg. Chem. 2015, 54, 3773−3780